Biogeochemical Layering and Transformation of Particulate Organic Carbon in the Tropical Northwestern Pacific Ocean Inferred from $\delta^{13}C$

Authors

Detong Tian[1,3], Xuegang Li[1,2,3,4*], Jinming Song[1,2,3,4*], Jun Ma[1,2], Huamao Yuan[1,2,3,4], Liqin Duan[1,2,3,4]

Affiliations

[1]CAS Key Laboratory of Marine Ecology and Environmental Sciences, Institute of Oceanology, Chinese Academy of Sciences, Qingdao 266000, China

[2]Laboratory for Marine Ecology and Environmental Science, Qingdao Marine Science and Technology Center, Qingdao 266237, China

[3]University of Chinese Academy of Sciences, Beijing 100049, China

[4]Center for Ocean Mega-Science, Chinese Academy of Sciences, Qingdao 266000, China

Corresponding to: Xuegang Li (lixuegang@qdio.ac.cn) and Jinming Song (jmsong@qdio.ac.cn).

Abstract. Particulate organic carbon (POC) serves as the main carrier of the biological pump and determines its transmission efficiency, yet the transformation processes of POC remain incompletely understood. This study reports the vertical distribution of POC, dissolved inorganic carbon (DIC), $\delta^{13}C$-POC, and $\delta^{13}C$-DIC in the tropical Northwestern Pacific Ocean (TNPO). The research identified three distinct biogeochemical layers governing POC transformation: the POC rapid synthesis-degradation layer (RSDL, 0-300 m), the net degradation layer (NDL, 300-1,000 m), and the stable layer (SL, 1,000-2,000 m). From the top to the bottom of the RSDL, $\delta^{13}C$-POC values decreased by an average of 2.23‰, while the carbon-to-nitrogen ratios (C:N) increased by an average of 2.3:1, indicating the selective degradation of POC. In the NDL, $\delta^{13}C$-POC and $\delta^{13}C$-DIC exhibited a significant negative correlation (r = 0.43, p < 0.05), indicating a net transformation of POC to DIC. In the SL, POC proved to be resistant to degradation, with POC exhibiting the highest C:N (15:1 on average) and the lowest $\delta^{13}C$-POC values (average -27.71‰).

1 Introduction

As the most significant carbon reservoir on the earth's surface, the ocean absorbs about 2.6 billion tons of carbon dioxide (CO_2) from the atmosphere each year, accounting for 25% of global anthropogenic CO_2 emissions (Friedlingstein et al., 2023). After entering the ocean, CO_2 initially dissolves in seawater, forming dissolved inorganic carbon (DIC). Subsequently, phytoplankton and photosynthetic bacteria at the ocean surface convert it into organic carbon through photosynthesis. The majority of carbon in the ocean is in the form of DIC, constituting over 98% of the total carbon content, with the remaining 2%

existing as POC and dissolved organic carbon (DOC). Despite being in minimal quantities, POC can be transported to the deep ocean through the biological pump and buried for thousands of years. This process of carbon sequestration aids in the absorption of CO_2 by the ocean, contributing to the regulation of atmospheric CO_2 levels (Longhurst and Glen Harrison, 1989; Turner, 2015). Organic matter produced from the euphotic layer is the primary food source for heterotrophic communities in the dark ocean (Smith et al., 2008); once POC is exported from the euphotic layer, microorganisms rapidly utilize it, releasing DIC (Song, 2010).

Some studies have shown that unstable components such as proteins and carbohydrates in POC are preferentially degraded by microorganisms (Eadie and Jeffrey, 1973). However, conducting detailed quantitative analyses of each POC component in actual investigations is challenging, necessitating the use of alternative indicators to demonstrate selective degradation. One generally accepted indicator is the carbon-to-nitrogen ratios (C:N) due to inherent differences in the C:N of various compounds in POC (Morales et al., 2021). Thus, changes in the C:N during degradation can signify the selective degradation of POC. Nevertheless, the composition of POC is highly complex, and the C:N of its different components are not absolute. For example, lipids typically have a higher C:N than proteins, but the opposite can also occur (Sannigrahi et al., 2005; Hernes and Benner, 2002). Therefore, relying solely on the C:N to reflect the selective degradation process of POC has significant limitations. Although the vital activities of the microbial community in the dark ocean are predominantly driven by heterotrophic respiration (Herndl et al., 2023), many autotrophic organisms use chemical energy to synthesize POC. Compelling evidence indicates that chemoautotrophy plays a substantial role in the fixation of DIC in the minimum oxygen zone (OMZ) (Reinthaler et al., 2010) and the deeper ocean (Passos et al., 2022; Walsh et al., 2009). Consequently, there is a continuous conversion of POC and DIC throughout the ocean water column. Exploring the degradation and synthesis of POC in the ocean is imperative to enhance our comprehension of the biological pump processes.

The DIC in seawater primarily occurs in four chemical forms: H_2CO_3, HCO_3^-, CO_3^{2-}, and CO_2. In comparison, the composition of POC is more complex. POC comprises various organic compounds originating from living organisms such as phytoplankton, zooplankton, and microorganisms. It also encompasses fecal particles, cell fragments, and diverse organic substances from external sources. Only a small fraction of the POC has been accurately identified in terms of molecular structures (Kharbush et al., 2020). As the depth increases, the readily degradable components in POC are used up, leading to a

more intricate structure of the remaining POC through the transformation process. The remaining refractory POC is even more difficult to identify (Lee et al., 2000). Therefore, it becomes challenging to study the chemical characteristics of POC and its transformation process from itself. The δ^{13}C is a crucial indicator that can reveal the origin, migration, and transformation of POC, making it significantly important in the investigation of the marine carbon cycle (Ding et al., 2020; Jeffrey et al., 1983). Compared with POC concentration, δ^{13}C-POC provides a more accurate reflection of the chemical properties of the POC pool and the migration and transformation processes of POC (Close and Henderson, 2020). Similarly, δ^{13}C-DIC can offer insights into important processes within the ocean carbon cycle. As POC settles, it undergoes a series of biogeochemical processes, including synthesis, degradation, and adsorption. Therefore, the isotope fractionation effect in POC is strong, resulting in significant differences in δ^{13}C-POC values at different depths. In contrast, the fractionation of δ^{13}C-DIC is subject to fewer influencing factors, and the DIC concentration in the ocean is notably high, thereby engendering minimal variability in δ^{13}C-DIC values across the ocean water column (Jeffrey et al., 1983). Therefore, δ^{13}C-DIC is more sensitive to the fractionation effect in the ocean carbon cycle. Even slight variations in the δ^{13}C-DIC values can reflect significant processes involved in the migration and transformation of POC (Quay and Stutsman, 2003). Through the analysis of δ^{13}C-POC and δ^{13}C-DIC values, we can enhance our comprehension of the intricate composition, transport, and alteration mechanism of POC, providing us with a more profound insight into the dynamic transformations within the ocean biological pump.

The tropical Northwestern Pacific Ocean (TNPO) is characterized by intricate current patterns and water mass distributions (Hu et al., 2015; Schönau et al., 2022), and it is also known for the highest surface seawater temperatures globally (Jia et al., 2018). High temperatures facilitate the respiration by heterotrophic organisms, promoting the formation of biological hotspots and ultimately enhancing material circulation and energy flow in the upper ocean (Guo et al., 2023a; Iversen and Ploug, 2013). The air-sea interaction within the TNPO is highly dynamic, exhibiting a shift from being a carbon sink to a carbon source as it extends from higher to lower latitudes (Takahashi et al., 2009; Wu et al., 2005). The complex hydrological characteristics, rapid elemental cycle, and frequent air-sea exchange render the TNPO an ideal laboratory for exploring the ocean carbon cycle. In this research, we collected seawater and particulate matter samples at six stations in the core and boundary regions of the TNPO,

93 and the relationship between DIC, POC, and their stable carbon isotopes was comprehensively analyzed

94 to enhance our understanding of the POC transformation process and the ocean carbon cycle process.

95 **2 Sampling and Methods**

96 The samples were collected in the TNPO during an expedition on R/V *Kexue* from March to April 2022.

97 A total of 6 stations were set up: EQ-6 (150.99° E, 0.00° N, 1944 m), E142-3 (140.99° E, 12.01° N, 4091

98 m), E142-7 (140.99° E, 15.99° N, 4725 m), E142-11 (140.99° E, 20.00° N, 462 4m), E142-13 (142.04°

99 E, 0.00° N, 3382 m) and E142-19 (141.99° E, 6.01° N, 2580 m) (Fig. 1). The 12-L Niskin bottles (KC-

100 Denmark, Denmark) mounted on a Conductivity-Temperature-Depth (CTD, Sea-bird SBE911, United

101 States) rosette were used to obtain water samples from the vertical profile of 0-2,000 m at each station

102 for analysis of temperature, salinity, dissolved oxygen (DO), POC, δ^{13}C-POC, particulate nitrogen (PN),

103 DIC, δ^{13}C-DIC, and chlorophyll a (Chl-*a*). The specific sampling and analysis methods are as follows.

104 **Temperature and salinity:** The temperature and salinity were measured by CTD (Sea-bird SBE911,

105 United States) in situ during sampling.

106 **DO:** DO was determined in situ using the Winkler method with a measurement precision of 2.2×10^{-3}

107 μmol/L. At each depth, we collected samples in 50 mL brown bottles, added manganese sulfate and

108 alkaline potassium iodide to fix the oxygen, then titrated the released iodine with sodium thiosulfate to

109 calculate DO concentrations (Bryan et al., 1976; Zuo et al., 2018). The discrete DO samples were used

110 to calibrate the DO concentration data obtained by the CTD sensor.

111 **POC, δ^{13}C-POC, and PN:** Particle samples were obtained by filtering 2-5 L of seawater onto a GF/F

112 glass filter (0.7 μm, Whatman) that had been combusted in a muffle furnace (450°C, 4 h) and acid-soaked

113 (0.5 M hydrochloric acid (HCl), 24 h). The filter was treated with HCl to remove inorganic carbonates

114 and oven-dried at 60°C. After collection, samples were stored below -20 °C until laboratory analysis.

115 Afterward, POC, PN concentration, and δ^{13}C-POC values were analyzed using an elemental analyzer

116 and an isotope mass spectrometer (Thermo Fisher Scientific Flash EA 1112 HT-Delta V Advantages,

117 United States) with an accuracy of ± 0.8‰ and ± 0.2‰, respectively. Standard reference materials were

118 used to calibrate δ^{13}C and POC, PN measurements, including USGS64 (δ^{13}C = -40.8 ± 0.04‰, C% =

119 31.97%, N% = 18.65%, Indiana University), USGS40 (δ^{13}C = -26.39 ± 0.04‰, C% = 40.8%, N% =

120 9.52%, Geological Survey, United States), and Urea #2a (δ^{13}C = -9.14 ± 0.02‰, C% = 20%, N% =

121   46.67%, Indiana University). We implemented a quality control protocol by randomly inserting a

122   certified reference material after every 10 samples. The measured values of these reference materials

123   were subsequently plotted against the calibration curve to monitor and verify instrument stability

124   throughout the analytical process (Ma et al., 2021).

125   **DIC and δ^{13}C-DIC:** Sampling was performed using a 50 ml glass bottle. After the water sample

126   overflowed, 1 ml of the sample was taken out with a pipette and then fixed with saturated mercuric

127   chloride solution to remove the influence of biological activity. After collection, samples were stored in

128   refrigerator at 4°C for later laboratory measurement of DIC concentration using a total DIC analyzer

129   (Apollo SciTech AS-C3, United States) with an accuracy of ± 0.1% (Ma et al., 2020). For calibration,

130   certified reference material (Batch 144, 2031.53 ± 0.62 μmol/kg) provided by the Scripps Institution of

131   Oceanography (University of California, San Diego) was used. δ^{13}C-DIC values **a**utomatic analysis was

132   performed using a Thermo Delta-V isotope ratio mass spectrometer (ThermoFisher Scientific MAT

133   253Plus, United States). For calibration, certified reference materials for δ^{13}C-DIC were used, including

134   GBW04498 (δ^{13}C = -27.28 ± 0.10‰), GBW04499 (δ^{13}C = -19.58 ± 0.10‰), and GBW04500 (δ^{13}C = -

135   4.58 ± 0.12‰), all provided by the Institute of Geophysical and Geochemical Exploration (Chinese

136   Academy of Geological Sciences). We inserted a reference standard every 10 samples, using its measured

137   values to verify instrument stability via the calibration curve.

138   **Chl -*a*:** 2 L of water sample after zooplankton removal was filtered onto pre-combusted (450°C for 5 h)

139   GF/F filters (0.7 μm, Whatman) and placed in the refrigerator at −20°C before measurement. In the

140   laboratory, the filters were extracted with 90% propanol for 12-24 h, and the concentration was measured

141   using a fluorescence photometer (Turner Designs, United States) For calibration, Chl-*a* analytical

142   standard (purity ≥ 95.0%) provided by Sigma-Aldrich (SIAL, St. Louis, MO, United States) was used.

143   (Ma et al., 2020).

144
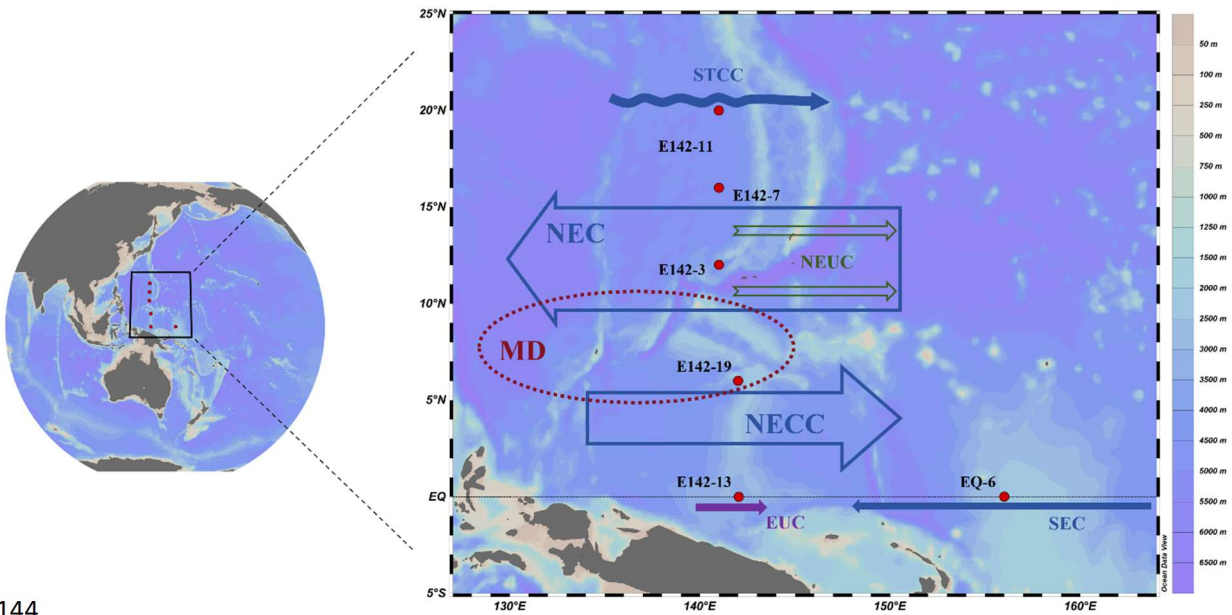
145 **Figure 1. TPWO sampling stations (red dots in the figure) and ocean current distribution. In the figure, blue**

146 **represents the ocean currents from the surface to the bottom of the thermocline, mainly STCC, NEC, NECC,**

147 **and SEC; green represents the ocean currents in the subthermocline, mainly NEUC; purple represents the**

148 **ocean currents from the bottom of the thermocline to the subthermocline, mainly EUC.**

149 **3 Results and Discussion**

150 **3.1 Hydrological Characteristics**

151 Except for station E142-11, the remaining five stations are all located at the Western Pacific Warm Pool

152 (WPWP). The SST of the five stations in the warm pool area was higher, averaging 29.01 ± 0.67 ℃,

153 while station E142-11 had a lower SST of 25.02 ℃. The strong seawater stratification in the study area

154 restricted the movement of nutrient-rich water from the deep to the upper ocean, resulting in the region

155 showing oligotrophic characteristics (Radenac et al., 2013). Therefore, the Chl-*a* concentration at the

156 deep chlorophyll maximum layer depth (DCMD) was low, with an average of only 0.24 ± 0.04 µg/L.

157 Based on the fluorescence intensity measured by the CTD in-situ fluorescence sensor, we calculated the

158 Primary Production Zone Depth (PPZD), which is the depth where the fluorescence intensity drops to

159 10% of its maximum value above this depth (Owens et al., 2015). Additionally, the Mixed Layer Depth

160 (MLD) at each station was determined using the temperature threshold method (Table 1) (Thompson,

161 1976). The results indicate that the PPZD at each station is deeper than the MLD, suggesting that the

162 POC generated at these stations does not undergo particularly complex physical mixing after its

163 formation (Buesseler et al., 2020).

Table 1. The water depth (WD), the PPZD, the MLD, the deep chlorophyll maximum layer depth (DCMD) and the Chl-*a* at DCMD for each station.

Station	Longitude °E	Latitude °N	WD m	PPZD m	MLD m	DCMD m	Chl-*a* μg/L
EQ-6	155.99	0.00	1944	129	65	50	0.31
E142-3	141.00	12.01	4091	216	102	140	0.19
E142-7	141.00	16.00	4725	204	68	150	0.25
E142-11	140.99	20.00	4624	203	42	90	0.21
E142-13	142.04	0.00	3382	165	45	90	0.25
E142-19	142.00	6.01	2580	170	109	100	0.21

Based on the relationship between potential temperature and salinity (θ-S) (Fig. 2), eight water masses in the study area were identified: North Pacific Tropical Surface Water (NPTSW), North Pacific Subsurface Water (NPSSW), North Pacific Subtropical Mode Water (NPSTMW), North Pacific Intermediate Water (NPIW), North Pacific Deep Water (NPDW), as well as Equatorial Surface Water (ESW), South Pacific Subsurface Water (SPSSW) and South Pacific Intermediate Water (SPIW). In the upper ocean (0-300 m), we found that both NPTSSW and SPSSW exhibited high salinity characteristics. The salinity of NPTSSW was distributed between 34.66 and 35.01, while the salinity of SPSSW was distributed between 35.15 and 35.65. In addition, as the water depth increased, the temperature of NPTSSW and SPSSW decreased significantly, with NPTSSW dropping from 27.18℃ to 16.21℃ and SPSSW dropping from 29.23℃ to 14.81℃. The representative water mass in the middle ocean (300-1000 m) is NPIW, which is characterized by a rapid decrease in temperature (11.44-5.57℃) and a slight increase in salinity (~0.3) with increasing water depth. The representative water mass in the deep ocean (1000-2000 m) is NPDW, which has stable properties and slight changes in salinity and temperature. Notably, the water mass distribution at station E142-19 is quite special. Ranging from the subsurface to the deep layer, the water mass properties of this station are relatively stable, showing low-salinity and low-temperature characteristics. This is attributed to the intrusion of both North Pacific Intermediate Water (NPIW) and South Pacific Intermediate Water (SPIW) into the station in the mid-ocean region. Additionally, the station is situated within the MD upwelling area, where strong upwelling transports low-temperature, low-salinity North Pacific Deep Water (NPDW) from the bottom to the upper layer, enhancing seawater exchange. Consequently, the water at station E142-19 comprises a mixture of diverse water masses (MW).
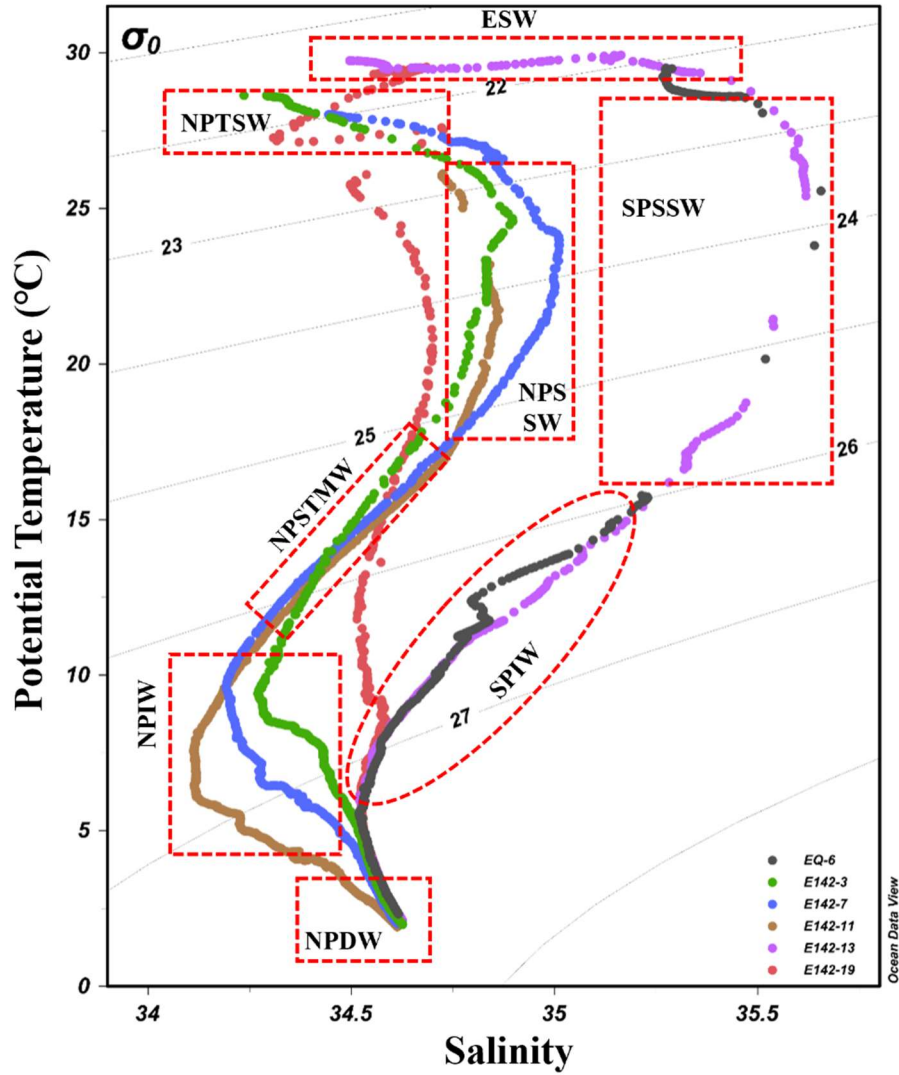
Figure 2. Relationship between potential temperature (θ) and salinity (S) at each sampling station. The water mass distribution is marked with a dotted line.

The study area is traversed by six major ocean currents: the South Equatorial Current (SEC), the North Equatorial Current (NEC), the North Equatorial Undercurrent (NEUC), the Subtropical Countercurrent (STCC), the Equatorial Undercurrent (EUC) and the North Equatorial Countercurrent (NECC). Among them, the SEC flows from east to west along the equator and is characterized by high temperature and low salinity, notably impacting station EQ-6. The NEC is a major westward current in the study area, accompanied by a series of eastward undercurrents of NEUC in its lower part; stations E142-3 and E142-7 are mainly affected by them. The STCC is characterized by a multi-eddy structure that flows eastward in the subtropical region of the North Pacific and notably impacts station E142-11. The EUC is a strong eastward current rich in oxygen and nutrients, which are present in the subsurface layer of the equatorial Pacific, forming the main body of the thermocline of this area; station E142-13 is deeply affected by it.

The NECC is an important current in the tropical Pacific equatorial current system, transporting warm pool water from the western Pacific to the eastern Pacific; Station E142-19 is mainly affected by it. Furthermore, the area features a substantial upwelling system known as the Mindanao Dome (MD), greatly impacting Station E142-19, situated southeast of the MD.

3.2 Vertical distribution characteristics of POC and δ^{13}C-POC

The average POC concentration from the surface to the deep chlorophyll maximum layer (DCM, 0-150 m) of the six stations was: E142-19 (34.12 ± 3.53 µg/L) > E142-13 (31.90 ± 3.19 µg/L) > EQ-6 (31.32 ± 5.27 µg/L) > E142-3 (27.77 ± 4.78 µg/L) > E142-7 (27.43 ± 1.35 µg/L) > E142-11 (26.81 ± 2.25 µg/L). Since the nutrient concentration in ESW and SPSSW is higher than that in NPTSW and NPTSSW, the surface POC concentrations at stations E142-13 and EQ-6 were slightly higher than those at other stations. However, the surface POC concentration at station E142-19 was the highest among the six stations because the robust upwelling of MD brought rich nutrients to the surface seawater, alleviating the nitrogen nutrient limitation of the surface water at this station (Gao et al., 2021).

The POC concentration of each station demonstrated a decreasing trend with increasing water depth and tended to remain stable in the deep ocean (> 1,000 m) (. The most significant drop in POC concentration occurred between the DCM and 600 m (Fig. 3). The seawater within this depth range was abundant in POC and also exhibited relatively high temperature and DO concentration, which likely enhanced the metabolic activities of heterotrophic organisms, thereby accelerating their utilization of POC (Iversen and Ploug, 2013; Sun et al., 2021). The aerobic degradation of POC led to a significant consumption of DO. Therefore, the change in DO in this water layer was consistent with the change of POC concentration (Fig. 3). It could be inferred that the rapid degradation of POC contributes to the accelerated formation of the oxygen cline. Since the microbial life activities below the oxygen cline were still active, leading to the continued consumption of DO through POC degradation, the DO could not be replenished in time. As a result, the low oxygen zone (where DO < 100 µmol/L) emerged in the middle ocean at all stations (Fig. 3). However, the hypoxic conditions observed at station E142-13 were comparatively less pronounced than those observed at other stations (Fig. 3). This can be attributed to the consistent transport of oxygen and nutrient-rich seawater by the EUC to this station, facilitating oxygen replenishment and mitigating deoxygenation (Brandt et al., 2021).

228
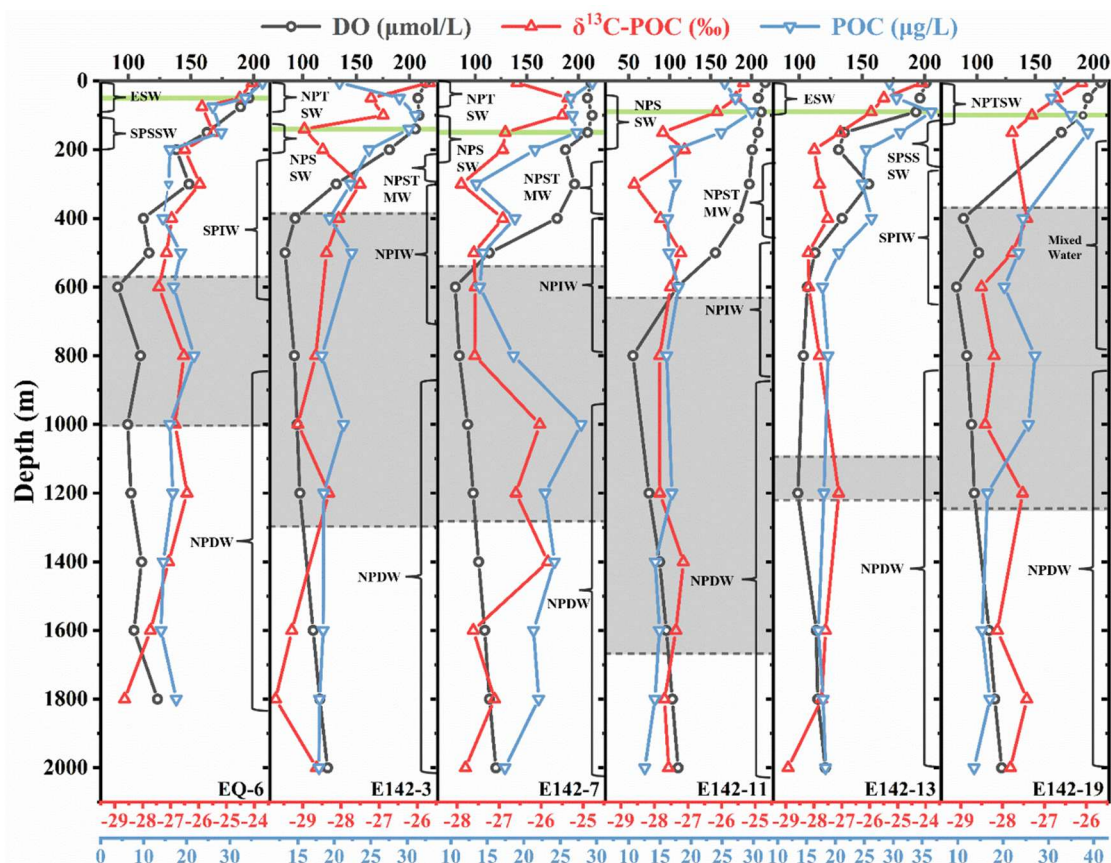
Figure 3. Vertical distribution of DO concentration, δ¹³C-POC values, and POC concentration at each sampling station. The gray area marks the hypoxic zone with DO = 100 μmol/L as the boundary. The green line represents the DCM depth.

The vertical distribution of δ^{13}C-POC values closely resembles that of POC concentration (Figs. 2, 3a). This similarity suggests that specific ^{13}C-enriched components may be preferentially degraded during POC degradation. Although the molecular composition of oceanic POC cannot be fully identified, it is generally understood to primarily consist of lipids, amino acids, carbohydrates, nucleic acids, and a small number of heterogeneous components (Kharbush et al., 2020). The metabolic activity of amino acids and carbohydrates is higher than lipids, leading microorganisms to preferentially use these compounds as energy sources, enriching lipids in POC (Hwang et al., 2006; Jeffrey et al., 1983). Previous studies have reported that during the degradation of POC, the carbon isotope fractionation characteristics of amino sugar monomers closely align with changes in δ^{13}C-POC values   (Guo et al., 2023b). Moreover, several studies have highlighted that the carbon isotopic composition of lipid monomers does not exhibit significant depletion during POC degradation; in fact, it may even show a trend of enrichment (Close et al., 2014; Häggi et al., 2021). These observations further indicate the preferential degradation of amino acids and carbohydrates in POC. On the other hand, compared with lipids, amino acids and carbohydrates

exhibit higher $\delta^{13}C$ values (Hayes, 1993; Hwang and Druffel, 2003; Schouten et al., 1998). When large

quantities of amino acids and carbohydrates undergo selective degradation, the residual POC will show

low $\delta^{13}C$ value characteristics. Therefore, as POC is continuously consumed in the water column, the

$\delta^{13}C$-POC values will gradually decrease. In addition, lipids have a low nitrogen content in comparison

to amino acids and carbohydrates, leading to a relatively high C:N (Morales et al., 2021). Our findings

demonstrated a strong negative correlation between $\delta^{13}C$-POC values and C:N (Fig. 4b), which implied

that as the water depth increases, $\delta^{13}C$-POC values decreases while the C:N in the remaining POC

increases. This suggests that selective degradation of POC occurs, during which amino acids and

carbohydrates in the POC were preferentially removed, resulting in a relative increase in the proportion

of lipids in the remaining POC (Druffel et al., 2003; Guo et al., 2023a). However, it is noteworthy that

in the upper ocean (0-300 m), although there is a significant negative correlation between $\delta^{13}C$-POC

values and C:N ratios ($p<0.05$), no significant correlation is observed between $\delta^{13}C$-POC values and POC

concentration ($p>0.05$) (Fig. 4a). This suggests that the fractionation of $\delta^{13}C$-POC at this depth layer is

not entirely controlled by selective degradation. Photosynthesis exerts a certain influence on the

fractionation of $\delta^{13}C$-POC within this depth range, primarily manifested as an increase in photosynthetic

carbon isotope fractionation with depth, leading to a decrease in $\delta^{13}C$-POC values. In a study conducted

in the subtropical North Atlantic, the photosynthetic carbon isotope fractionation increased by 5.6‰ from

the upper to the lower euphotic zone, while the $\delta^{13}C$ values of the photosynthetic product, phytol,

decreased by 6.3‰ (Henderson et al., 2024). Therefore, although the process of selective degradation

significantly affects the fractionation of $\delta^{13}C$-POC, it is still necessary to consider the regulatory effects

of other processes in certain unique marine environments.
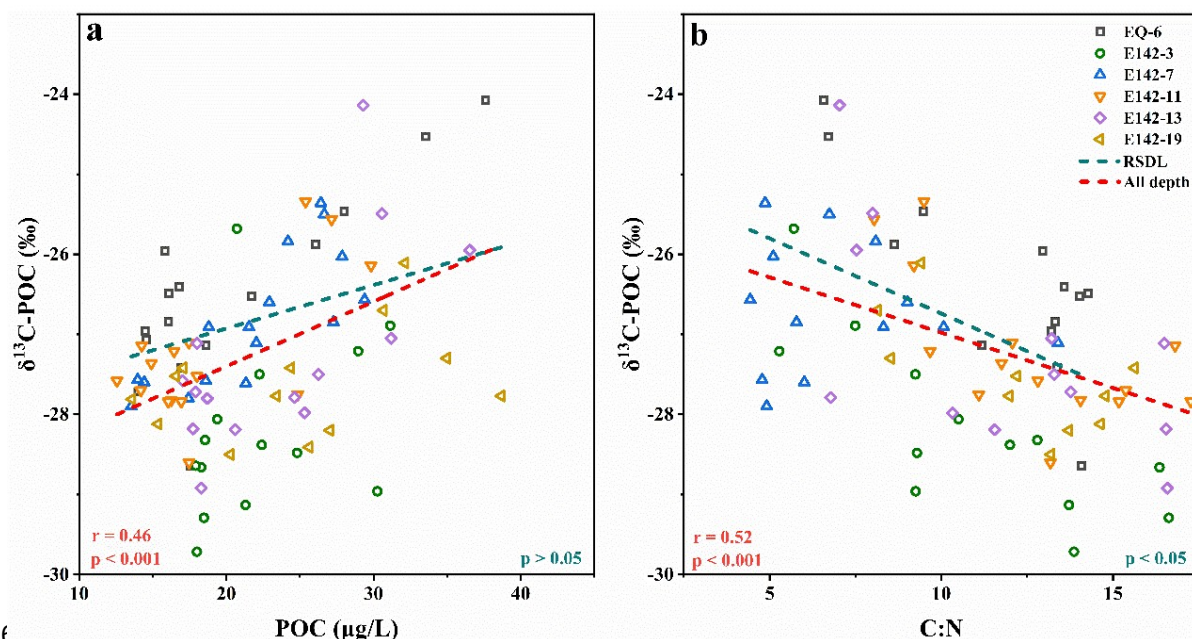
Figure 4. a. Relationship between δ¹³C-POC values and POC concentration; b. Relationship between δ¹³C-POC values and C:N

3.3 Vertical distribution characteristics of DIC and δ¹³C-DIC

Among the six stations, only the equatorial stations E143-13 and EQ-6 exhibited average upper DIC concentrations exceeding 2000 μmol/kg, with values of 2036 and 2054 μmol/kg, respectively. This phenomenon can be attributed to the fact that the surface water masses at these stations are composed of high-temperature and high-salinity ESW (Fig. 2). Although high temperatures generally hinder the dissolution of CO_2, they can accelerate the rate of CO_2 release by heterotrophic organisms. Meanwhile, high salinity increases the ionic strength and buffering capacity of seawater, promoting DIC accumulation (Zeebe and Wolf-Gladrow, 2001). These factors collectively contribute to the high DIC concentrations observed in the surface layers of these two stations. The average upper DIC concentration at station E142-19 was the next highest, reaching 1992 μmol/kg. This is due to upwelling at this station, which transports deep, high-DIC seawater to the middle ocean. Consequently, this station also recorded the highest average mid-layer DIC concentration among the six stations, at 2184 μmol/kg. Furthermore, since stations E142-3, E142-7, and E142-11 are predominantly influenced by the same water mass across all depths, their DIC concentrations are relatively similar at each depth (Fig. 5). The average DIC concentrations of all six stations in the upper ocean, middle ocean, and deep ocean were 2004 ± 65, 2147 ± 35, and 2234 ± 26 μmol/kg, respectively. There was a significant increase in DIC concentration from the upper to the deep ocean (Fig. 5). Affected by photosynthesis, DIC increases gradually in the upper

ocean. In contrast, in the middle ocean, the rapid decomposition of POC released a large amount of

inorganic carbon, causing a rapid increase in DIC throughout the water column. Then, in the deep ocean,

a small amount of POC continues to degrade, while the release of DIC due to decreasing carbonate

saturation with depth contributes to a gradual increase in DIC concentration within this layer.

Moreover, we observed surface δ^{13}C-DIC values ranging from -0.55 to 0.45‰ (average 0.12‰) in the

research region, which is significantly lower than those reported in studies conducted in the Pacific region

in the 1990s (Quay et al., 2017; Quay and Stutsman, 2003). This suggests that the ocean has absorbed

more anthropogenic CO_2 as atmospheric CO_2 concentrations have increased over the years. The surface

δ^{13}C-DIC value of station E142-11 was the lowest among the six stations, only -0.55‰, while the surface

δ^{13}C-DIC value of station EQ-6 was the highest among the six stations, reaching 0.45‰. This is because

station E142-11 was located at the strongest atmospheric CO_2 net sink area, while station EQ-6 was

located at the atmospheric CO_2 net source area (Zhong et al., 2022). The sea-air exchange at station

E142-11 was sufficient, leading to a lower δ^{13}C-DIC value in its surface water, as it was more likely to

reach isotopic equilibrium with atmospheric CO_2. In contrast, the surface water of station EQ-6 was more

susceptible to seawater mixing and biological primary production influences. The higher δ^{13}C-DIC

values observed in the surface water of station EQ-6 can be attributed to the isotope fractionation caused

by the consumption of a substantial amount of CO_2 by biological primary production (Quay et al., 2003).

In analyzing the vertical distribution of δ^{13}C-DIC, the findings revealed a rapid decrease in δ^{13}C-DIC

values at each station, mirroring the decline seen in δ^{13}C-POC values in the upper ocean (0-300 m) (Figs.

4, 5d). Within this depth range, the average decrease in δ^{13}C-POC values was 2.23‰, while the average

decrease of δ^{13}C-DIC values was 0.30‰, with δ^{13}C-DIC reaching its minimum value in the subsurface.

However, in the middle ocean layer (300-1,000 m), unlike δ^{13}C-POC, δ^{13}C-DIC values increased first

and then stabilized (Fig. 5). Therefore, distinct differences exist in the overall change trends of δ^{13}C-DIC

values and δ^{13}C-POC values in the ocean water column. Since the mutual conversion between POC and

DIC was ongoing, this conversion process will inevitably cause changes in δ^{13}C-POC and δ^{13}C-DIC.

Generally, the variation range of δ^{13}C-POC values was more significant than that of δ^{13}C-DIC values,

indicating the more complex biogeochemical processes experienced by POC (Meyer et al., 2016;

Schmittner et al., 2013). This difference is also partly due to the much larger size of the DIC pool

compared to the POC pool (Jeffrey et al., 1983). The high DIC concentration in the ocean buffers its

isotopic variability, resulting in minimal changes in δ^{13}C-DIC values across the water column, whereas

316 the smaller POC pool is more sensitive to localized biogeochemical processes, leading to greater

317 variability in δ^{13}C-POC values.

318

319
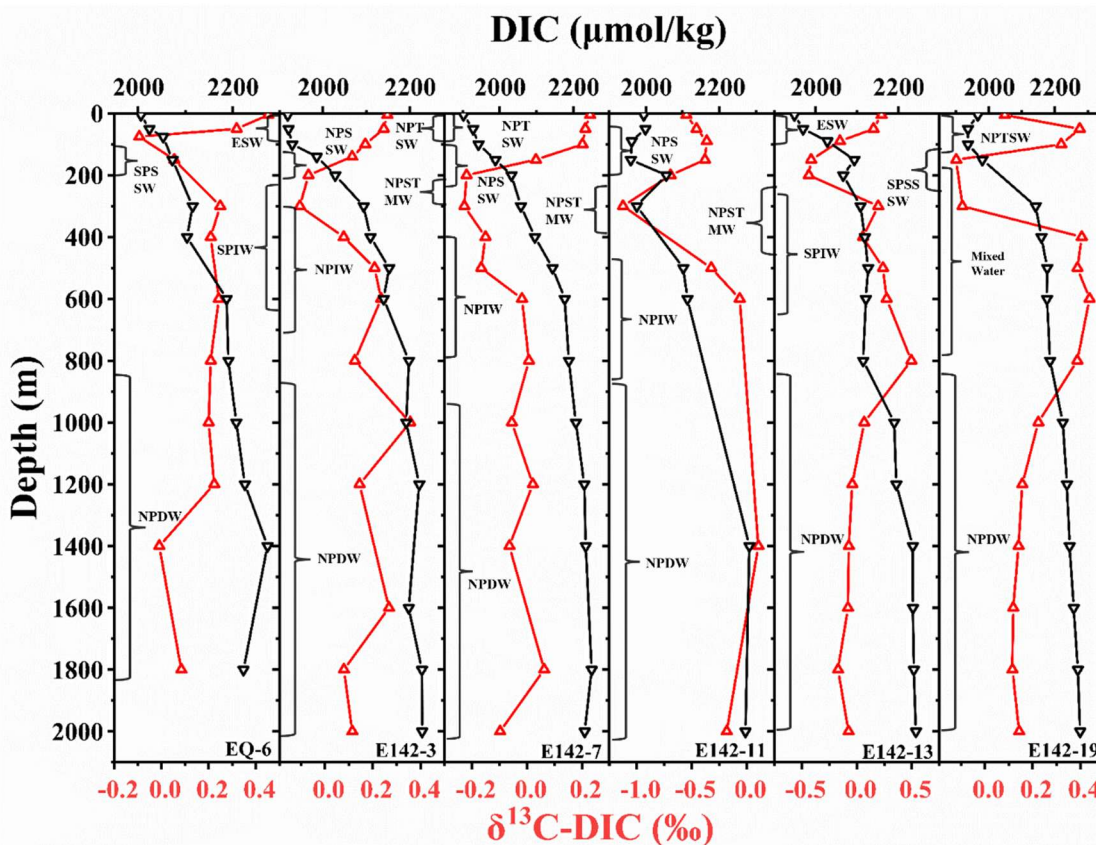
320 **Figure 5. Vertical distribution of DIC concentration and δ^{13}C-DIC values at each sampling station. The black**

321 **line represents DIC, and the red line represents δ^{13}C-DIC.**

322 **3.4 Transformation characteristics of POC in different water layers**

323 According to the distribution characteristics of δ^{13}C-POC and δ^{13}C-DIC values, we divided the ocean

324 water column into three biogeochemical layers: the POC rapid synthesis-degradation layer (RSDL, 0-

325 300 m), the net degradation layer (NDL, 300-1,000 m) and the stable layer (SL, 1,000-2,000 m). Within

326 the RSDL, POC was rapidly degraded while being synthesized. The synthesis of POC likely exceeded

327 its degradation from the surface to the DCM layer, while the degradation of POC appeared to dominate

328 below the DCM. In this layer, the δ^{13}C-POC values and C:N exhibited a pronounced negative correlation,

329 while no significant correlation is observed between δ^{13}C-POC values and POC concentration ($p > 0.05$)

330 (Figs. 4a, 6a). Therefore, the rapid decrease of δ^{13}C-POC values in this layer was dominated by the

331 selective degradation of POC and photosynthesis. Both δ^{13}C-POC and δ^{13}C-DIC values decrease with

332 increasing depth in the RSDL (Figs. 3, 5), and they exhibit a significant positive correlation within this

333   layer (Fig. 6d). Although the degradation of POC typically lowers the $\delta^{13}C$ value of DIC, as the $\delta^{13}C$

334   value of POC is lower than that of DIC, the significant decline in $\delta^{13}C$-DIC values observed in the RSDL,

335   when considering the substantial difference in magnitude between the POC pool and the DIC pool,

336   suggests the influence of additional processes. Specifically, the phytoplankton and photosynthetic

337   bacteria in the upper ocean tended to use the light $^{12}CO_2$ in the seawater for photosynthesis; thus the

338   $\delta^{13}C$-DIC values of the surface ocean at all stations was relatively high. However, light intensity

339   diminishes with increasing depth, which is unfavorable for photosynthesis. This leads to the

340   accumulation of $^{12}CO_2$ produced by the respiration of heterotrophic communities. Consequently, the

341   $\delta^{13}C$-DIC values in this layer steadily declined (Ge et al., 2022). In the NDL, sunlight was extremely

342   weak, and photosynthesis was nearly absent. Heterotrophic communities dominate, leading to a

343   continuous decrease in POC concentration and a corresponding increase in DIC concentration (Figs. 3,

344   5). Generally, the degradation of POC would be expected to lower the $\delta^{13}C$ value of DIC. However, in

345   this layer, $\delta^{13}C$-POC values showed a significant negative correlation with both C:N and $\delta^{13}C$-DIC values

346   (Fig. 6b, e), indicating the influence of additional processes on $\delta^{13}C$-DIC fractionation. The NDL often

347   encompasses low-oxygen zones (Fig. 3), which are known to favor the activity of chemoautotrophic

348   microorganisms. Compared to aerobic environments, the energy required for microorganisms to fix

349   inorganic carbon into organic carbon is lower under low-oxygen condition (Hugler and Sievert, 2011;

350   Mccollom and Amend, 2005). During this process, chemoautotrophic microorganisms preferentially

351   utilize lighter ^{12}C isotopes, leading to the enrichment of ^{13}C in the remaining DIC pool. This microbial

352   activity explains the observed increase in $\delta^{13}C$-DIC values in the NDL. In the SL, the POC concentration

353   remained consistently low. $\delta^{13}C$-POC values did not correlate significantly with either C:N or $\delta^{13}C$-DIC

354   (Fig. 6c, f). This was because the easily degradable components in POC had been completely consumed

355   in the RSDL and NDL, and the remaining components were relatively refractory. As a result, the

356   conversion of POC to DIC was rare in SL, leading to an absence of a clear link between $\delta^{13}C$-POC and

357   $\delta^{13}C$-DIC.

358
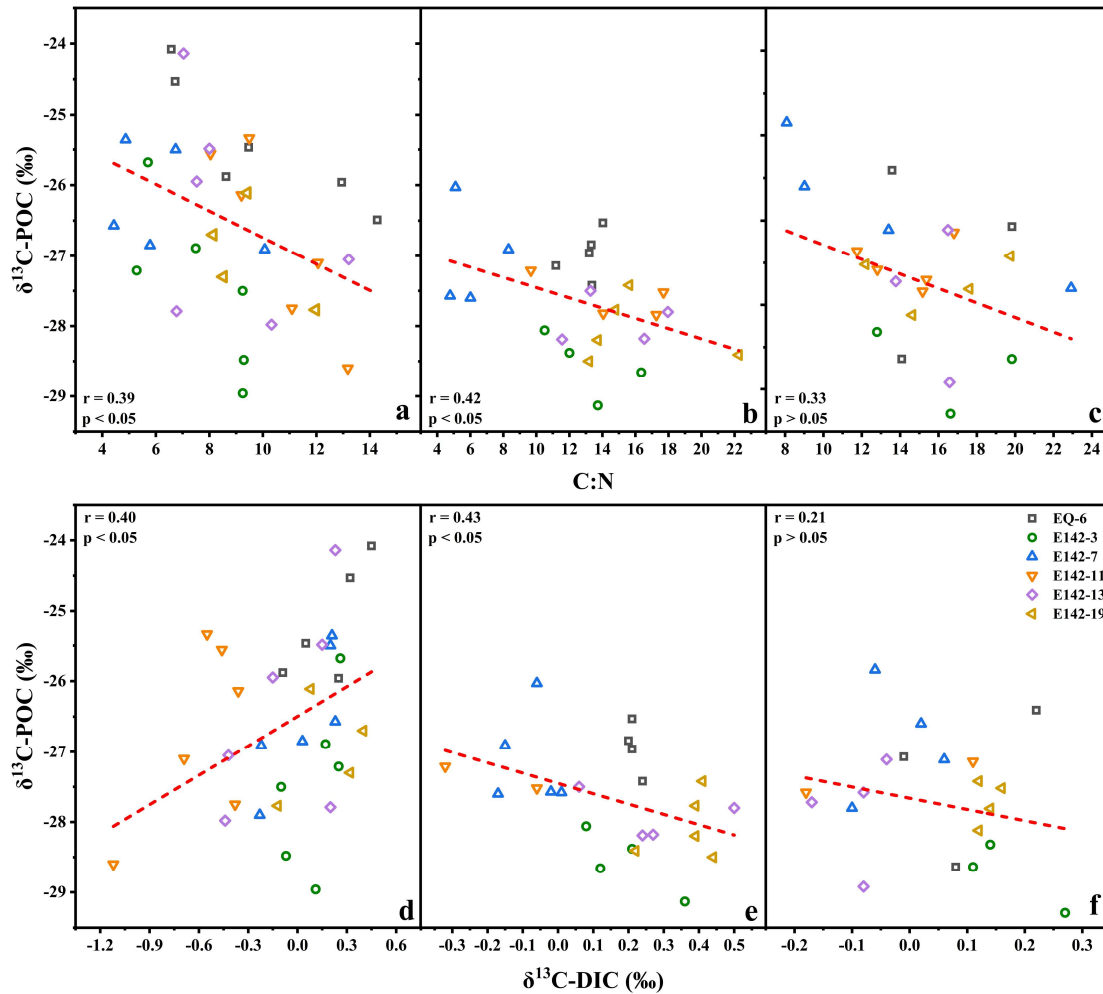
359 **Figure 6. Relationships between δ¹³C-POC and C:N at different depths: (a) 0-300 m, (b) 300-1,000 m, (c)**

360 **1,000-2,000 m, and between δ¹³C-POC and δ¹³C-DIC at different depths: (d) 0-300 m, (e) 300-1,000 m, (f)**

361 **1,000-2,000 m.**

362 **4 Conclusions**

363 In general, this study investigated the transformation characteristics of POC in the tropical northwest

364 Pacific Ocean based on the δ¹³C perspective. Our findings revealed three distinct stages of POC behavior

365 in the ocean: rapid synthesis-degradation, net degradation, and stable existence. Below the RSDL, the

366 selective degradation of POC dominated the changes in δ¹³C-POC. The C:N ratio data in RSDL and NDL

367 indicate an increase in the proportion of refractory lipids in POC, relative to more labile components

368 such as amino acids and carbohydrates. Consequently, in the SL, POC was found to be stable with a slow

369 degradation rate. The fractionation of δ¹³C-DIC in the ocean is influenced by both the production and

370 degradation processes of POC. Within the RSDL, δ¹³C-DIC fractionation is predominantly governed by

371 primary production, whereas within the NDL and SL, it is primarily influenced by the degradation

372 process of POC.

373 Although we utilized δ^{13}C-POC and δ^{13}C-DIC to assess the overall transformation characteristics of POC,

374 the specific synthesis and decomposition ratios of POC are still challenging to determine. Further

375 research is needed on the monomer carbon isotopic composition of POC (lipids, amino acids, etc.) to

376 enhance our understanding of the transformation process of POC.

377 **Data Availability.** The data files used in this paper are available at (Tian et al., 2024).

378 **Competing interest.** The authors declare that they have no conflict of interest.

379 **Author contribution.** Detong Tian: Investigation, Data Curation, Writing-original draft. Xuegang Li
380 and Jinming Song: Conceptualization, Funding acquisition, Writing-review & editing. Jun Ma, Funding
381 acquisition. Huamao Yuan, Liqin Duan: Writing - Review & Editing.

382 **Acknowledgments.** This work was supported by the National Key Research and Development Program
383 (grant no. 2022YFC3104305), National Natural Science Foundation of China (grant nos.42176200,
384 42206135); Laoshan Laboratory (grant nos. LSKJ202204001, LSKJ202205001). We appreciate the
385 crews of the R/V *Kexue* for sampling assistance during the cruise of NORC2021-09 supported by the
386 National Natural Science Foundation of China (project no. 42049909).

References

Brandt, P., Hahn, J., Schmidtko, S., Tuchen, F. P., Kopte, R., Kiko, R., Bourlès, B., Czeschel, R., and Dengler, M.: Atlantic Equatorial Undercurrent intensification counteracts warming-induced deoxygenation, Nat. Geosci., 14, 278-282, http://doi.org/10.1038/s41561-021-00716-1, 2021.

Bryan, J. R., Rlley, J. P., and Williams, P. J. L.: A winkler procedure for making precise measurements of oxygen concentration for productivity and related studies, Journal of Experimental Marine Biology and Ecology, 21, 191-197, http://doi.org/10.1016/0022-0981 (76)90114-3, 1976.

Buesseler, K. O., Boyd, P. W., Black, E. E., and Siegel, D. A.: Metrics that matter for assessing the ocean biological carbon pump, Proc Natl Acad Sci U S A, 117, 9679-9687, http://doi.org/10.1073/pnas.1918114117, 2020.

Close, H. G. and Henderson, L. C.: Open-Ocean Minima in $\delta^{13}C$ Values of Particulate Organic Carbon in the Lower Euphotic Zone, Front. Mar. Sci., 7, http://doi.org/10.3389/fmars.2020.540165, 2020.

Close, H. G., Wakeham, S. G., and Pearson, A.: Lipid and ^{13}C signatures of submicron and suspended particulate organic matter in the Eastern Tropical North Pacific: Implications for the contribution of Bacteria, Deep Sea Res. Part I Oceanogr. Res. Pap., 85, 15-34, http://doi.org/10.1016/j.dsr.2013.11.005, 2014.

Ding, L., Qi, Y., Shan, S., Ge, T., Luo, C., and Wang, X.: Radiocarbon in Dissolved Organic and Inorganic Carbon of the South China Sea, J. Geophys. Res. Oceans, 125, http://doi.org/10.1029/2020jc016073, 2020.

Druffel, E. R. M., Bauer, J. E., Griffin, S., and Hwang, J.: Penetration of anthropogenic carbon into organic particles of the deep ocean, Geophys. Res. Lett., 30, http://doi.org/10.1029/2003gl017423, 2003.

Eadie, B. J. and Jeffrey, L. M.: $\delta^{13}C$ analyses of oceanic particulate organic matter, Mar. Chem., 1, 199-209, http://doi.org/10.1016/0304-4203 (73)90004-2, 1973.

Friedlingstein, P., O'Sullivan, M., Jones, M. W., Andrew, R. M., Bakker, D. C. E., Hauck, J., Landschützer, P., Le Quéré, C., Luijkx, I. T., Peters, G. P., Peters, W., Pongratz, J., Schwingshackl, C., Sitch, S., Canadell, J. G., Ciais, P., Jackson, R. B., Alin, S. R., Anthoni, P., Barbero, L., Bates, N. R., Becker, M., Bellouin, N., Decharme, B., Bopp, L., Brasika, I. B. M., Cadule, P., Chamberlain, M. A., Chandra, N., Chau, T.-T.-T., Chevallier, F., Chini, L. P., Cronin, M., Dou, X., Enyo, K., Evans, W., Falk, S., Feely, R. A., Feng, L., Ford, D. J., Gasser, T., Ghattas, J., Gkritzalis, T., Grassi, G., Gregor, L., Gruber, N., Gürses, Ö., Harris, I., Hefner, M., Heinke, J., Houghton, R. A., Hurtt, G. C., Iida, Y., Ilyina, T., Jacobson, A. R., Jain, A., Jarníková, T., Jersild, A., Jiang, F., Jin, Z., Joos, F., Kato, E., Keeling, R. F., Kennedy, D., Klein Goldewijk, K., Knauer, J., Korsbakken, J. I., Körtzinger, A., Lan, X., Lefèvre, N., Li, H., Liu, J., Liu, Z., Ma, L., Marland, G., Mayot, N., McGuire, P. C., McKinley, G. A., Meyer, G., Morgan, E. J., Munro, D. R., Nakaoka, S.-I., Niwa, Y., O'Brien, K. M., Olsen, A., Omar, A. M., Ono, T., Paulsen, M., Pierrot, D., Pocock, K., Poulter, B., Powis, C. M., Rehder, G., Resplandy, L., Robertson, E., Rödenbeck, C., Rosan, T. M., Schwinger, J., Séférian, R., Smallman, T. L., Smith, S. M., Sospedra-Alfonso, R., Sun, Q., Sutton, A. J., Sweeney, C., Takao, S., Tans, P. P., Tian, H., Tilbrook, B., Tsujino, H., Tubiello, F., van der Werf, G. R., van Ooijen, E., Wanninkhof, R., Watanabe, M., Wimart-Rousseau, C., Yang, D., Yang, X., Yuan, W., Yue, X., Zaehle, S., Zeng, J., and Zheng, B.: Global Carbon Budget 2023, Earth Syst. Sci. Data, 15, 5301-5369, http://doi.org/10.5194/essd-15-5301-2023, 2023.

Gao, W., Wang, Z., Li, X., and Huang, H.: The increased storage of suspended particulate matter in the upper water of the tropical Western Pacific during the 2015/2016 super El Niño event, J. Oceanol.

431   Limnol., 39, 1675-1689, http://doi.org/10.1007/s00343-021-0362-0, 2021.

432 Ge, T., Luo, C., Ren, P., Zhang, H., Fan, D., Chen, H., Chen, Z., Zhang, J., and Wang, X.: Stable carbon

433   isotopes of dissolved inorganic carbon in the Western North Pacific Ocean: Proxy for water mixing

434   and dynamics, Front. Mar. Sci., 9, http://doi.org/10.3389/fmars.2022.998437, 2022.

435 Guo, J., Zhou, B., Achterberg, E. P., Yuan, H., Song, J., Duan, L., and Li, X.: Rapid Cycling of Bacterial

436   Particulate Organic Matter in the Upper Layer of the Western Pacific Warm Pool, Geophys. Res.

437   Lett., 50, http://doi.org/10.1029/2023gl102896, 2023a.

438 Guo, J., Achterberg, E. P., Shen, Y., Yuan, H., Song, J., Liu, J., Li, X., and Duan, L.: Stable carbon isotopic

439   composition of amino sugars in heterotrophic bacteria and phytoplankton: Implications for

440   assessment of marine organic matter degradation, Limnology and Oceanography, 68, 2814-2825,

441   http://doi.org/10.1002/lno.12468, 2023b.

442 Häggi, C., Pätzold, J., Bouillon, S., and Schefuß, E.: Impact of selective degradation on molecular isotope

443   compositions in oxic and anoxic marine sediments, Org. Geochem., 153,

444   http://doi.org/10.1016/j.orggeochem.2021.104192, 2021.

445 Hayes, J. M.: Factors controlling ^{13}C contents of sedimentary organic compounds: Principles and

446   evidence, Mar. Geol., 113, 111-125, http://doi.org/10.1016/0025-3227 (93)90153-m, 1993.

447 Henderson, L. C., Wittmers, F., Carlson, C. A., Worden, A. Z., and Close, H. G.: Variable carbon isotope

448   fractionation of photosynthetic communities over depth in an open-ocean euphotic zone, Proc Natl

449   Acad Sci U S A, 121, e2304613121, http://doi.org/10.1073/pnas.2304613121, 2024.

450 Herndl, G. J., Bayer, B., Baltar, F., and Reinthaler, T.: Prokaryotic Life in the Deep Ocean's Water Column,

451   Ann Rev Mar Sci, 15, 461-483, http://doi.org/10.1146/annurev-marine-032122-115655, 2023.

452 Hernes, P. J. and Benner, R.: Transport and diagenesis of dissolved and particulate terrigenous organic

453   matter in the North Pacific Ocean, Deep Sea Res. Part I Oceanogr. Res. Pap., 49, 2119-2132,

454   http://doi.org/10.1016/s0967-0637 (02)00128-0, 2002.

455 Hu, D., Wu, L., Cai, W., Gupta, A. S., Ganachaud, A., Qiu, B., Gordon, A. L., Lin, X., Chen, Z., Hu, S.,

456   Wang, G., Wang, Q., Sprintall, J., Qu, T., Kashino, Y., Wang, F., and Kessler, W. S.: Pacific western

457   boundary currents and their roles in climate, Nature, 522, 299-308,

458   http://doi.org/10.1038/nature14504, 2015.

459 Hugler, M. and Sievert, S. M.: Beyond the Calvin cycle: autotrophic carbon fixation in the ocean, Ann

460   Rev Mar Sci, 3, 261-289, http://doi.org/10.1146/annurev-marine-120709-142712, 2011.

461 Hwang, J. and Druffel, E. R.: Lipid-like material as the source of the uncharacterized organic carbon in

462   the ocean?, Science, 299, 881-884, http://doi.org/10.1126/science.1078508, 2003.

463 Hwang, J., Druffel, E. R. M., Eglinton, T. I., and Repeta, D. J.: Source (s) and cycling of the

464   nonhydrolyzable organic fraction of oceanic particles, Geochim. Cosmochim. Acta, 70, 5162-5168,

465   http://doi.org/10.1016/j.gca.2006.07.020, 2006.

466 Iversen, M. H. and Ploug, H.: Temperature effects on carbon-specific respiration rate and sinking velocity

467   of diatom aggregates – potential implications for deep ocean export processes, Biogeosciences, 10,

468   4073-4085, http://doi.org/10.5194/bg-10-4073-2013, 2013.

469 Jeffrey, A. W. A., Pflaum, R. C., Brooks, J. M., and Sackett, W. M.: Vertical trends in particulate organic

470   carbon ^{13}C: ^{12}C ratios in the upper water column, Deep Sea Research Part A. Oceanographic

471   Research Papers, 30, 971-983, http://doi.org/10.1016/0198-0149 (83)90052-3, 1983.

472 Jia, Q., Li, T., Xiong, Z., Steinke, S., Jiang, F., Chang, F., and Qin, B.: Hydrological variability in the

473   western tropical Pacific over the past 700 kyr and its linkage to Northern Hemisphere climatic

474   change, Palaeogeogr. Palaeoclimatol. Palaeoecol., 493, 44-54,

475   http://doi.org/10.1016/j.palaeo.2017.12.039, 2018.

476   Kharbush, J. J., Close, H. G., Van Mooy, B. A. S., Arnosti, C., Smittenberg, R. H., Le Moigne, F. A. C.,

477   Mollenhauer, G., Scholz-Böttcher, B., Obreht, I., Koch, B. P., Becker, K. W., Iversen, M. H., and

478   Mohr, W.: Particulate Organic Carbon Deconstructed: Molecular and Chemical Composition of

479   Particulate Organic Carbon in the Ocean, Front. Mar. Sci., 7,

480   http://doi.org/10.3389/fmars.2020.00518, 2020.

481   Lee, C., Wakeham, S. G., and I. Hedges, J.: Composition and flux of particulate amino acids and

482   chloropigments in equatorial Pacific seawater and sediments, Deep Sea Res. Part I Oceanogr. Res.

483   Pap., 47, 1535-1568, http://doi.org/10.1016/s0967-0637 (99)00116-8, 2000.

484   Longhurst, A. R. and Glen Harrison, W.: The biological pump: Profiles of plankton production and

485   consumption in the upper ocean, Prog. Oceanogr., 22, 47-123, http://doi.org/10.1016/0079-6611

486   (89)90010-4, 1989.

487   Ma, J., Song, J., Li, X., Yuan, H., Li, N., Duan, L., and Wang, Q.: Control factors of DIC in the Y3

488   seamount waters of the Western Pacific Ocean, J. Oceanol. Limnol., 38, 1215-1224,

489   http://doi.org/10.1007/s00343-020-9314-3, 2020.

490   Ma, J., Song, J., Li, X., Wang, Q., Zhong, G., Yuan, H., Li, N., and Duan, L.: The OMZ and Its Influence

491   on POC in the Tropical Western Pacific Ocean: Based on the Survey in March 2018, Front. Earth

492   Sci., 9, http://doi.org/10.3389/feart.2021.632229, 2021.

493   McCollom, T. M. and Amend, J. P.: A thermodynamic assessment of energy requirements for biomass

494   synthesis by chemolithoautotrophic micro-organisms in oxic and anoxic environments, Geobiology,

495   3, 135-144, http://doi.org/10.1111/j.1472-4669.2005.00045.x, 2005.

496   Meyer, K. M., Ridgwell, A., and Payne, J. L.: The influence of the biological pump on ocean chemistry:

497   implications for long-term trends in marine redox chemistry, the global carbon cycle, and marine

498   animal ecosystems, Geobiology, 14, 207-219, http://doi.org/10.1111/gbi.12176, 2016.

499   Morales, M., Aflalo, C., and Bernard, O.: Microalgal lipids: A review of lipids potential and

500   quantification for 95 phytoplankton species, Biomass and Bioenergy, 150,

501   http://doi.org/10.1016/j.biombioe.2021.106108, 2021.

502   Owens, S. A., Pike, S., and Buesseler, K. O.: Thorium-234 as a tracer of particle dynamics and upper

503   ocean export in the Atlantic Ocean, Deep Sea Res. Part II Top. Stud. Oceanogr., 116, 42-59,

504   http://doi.org/10.1016/j.dsr2.2014.11.010, 2015.

505   Passos, J. G., Soares, L. F., Sumida, P. Y. G., Bendia, A. G., Nakamura, F. M., Pellizari, V. H., and Signori,

506   C. N.: Contribution of chemoautotrophy and heterotrophy to the microbial carbon cycle in the

507   Southwestern Atlantic Ocean, Ocean Coast. Res., 70, http://doi.org/10.1590/2675-

508   2824070.22137jgp, 2022.

509   Quay, P. and Stutsman, J.: Surface layer carbon budget for the subtropical N. Pacific: constraints at station

510   ALOHA, Deep Sea Res. Part I Oceanogr. Res. Pap., 50, 1045-1061, http://doi.org/10.1016/s0967-

511   0637 (03)00116-x, 2003.

512   Quay, P., Sonnerup, R., Munro, D., and Sweeney, C.: Anthropogenic CO_2 accumulation and uptake rates

513   in the Pacific Ocean based on changes in the $^{13}C/^{12}C$ of dissolved inorganic carbon, Glob.

514   Biogeochem. Cycles, 31, 59-80, http://doi.org/10.1002/2016gb005460, 2017.

515   Quay, P., Sonnerup, R., Westby, T., Stutsman, J., and McNichol, A.: Changes in the $^{13}C/^{12}C$ of dissolved

516   inorganic carbon in the ocean as a tracer of anthropogenic CO_2 uptake, Glob. Biogeochem. Cycles,

517   17, http://doi.org/10.1029/2001gb001817, 2003.

518   Radenac, M.-H., Messié, M., Léger, F., and Bosc, C.: A very oligotrophic zone observed from space in

the equatorial Pacific warm pool, Remote Sens. Environ., 134, 224-233, http://doi.org/10.1016/j.rse.2013.03.007, 2013.

Reinthaler, T., van Aken, H. M., and Herndl, G. J.: Major contribution of autotrophy to microbial carbon cycling in the deep North Atlantic's interior, Deep Sea Res. Part II Top. Stud. Oceanogr., 57, 1572-1580, http://doi.org/10.1016/j.dsr2.2010.02.023, 2010.

Sannigrahi, P., Ingall, E. D., and Benner, R.: Cycling of dissolved and particulate organic matter at station Aloha: Insights from ^{13}C NMR spectroscopy coupled with elemental, isotopic and molecular analyses, Deep Sea Res. Part I Oceanogr. Res. Pap., 52, 1429-1444, http://doi.org/10.1016/j.dsr.2005.04.001, 2005.

Schmittner, A., Gruber, N., Mix, A. C., Key, R. M., Tagliabue, A., and Westberry, T. K.: Biology and air–sea gas exchange controls on the distribution of carbon isotope ratios (δ¹³C) in the ocean, Biogeosciences, 10, 5793-5816, http://doi.org/10.5194/bg-10-5793-2013, 2013.

Schönau, M. C., Rudnick, D. L., Gopalakrishnan, G., Cornuelle, B. D., and Qiu, B.: Mean, Annual, and Interannual Circulation and Volume Transport in the Western Tropical North Pacific From the Western Pacific Ocean State Estimates (WPOSE), J. Geophys. Res. Oceans, 127, http://doi.org/10.1029/2021jc018213, 2022.

Schouten, S., Klein Breteler, W. C. M., Blokker, P., Schogt, N., Rijpstra, W. I. C., Grice, K., Baas, M., and Sinninghe Damsté, J. S.: Biosynthetic effects on the stable carbon isotopic compositions of algal lipids: implications for deciphering the carbon isotopic biomarker record, Geochim. Cosmochim. Acta, 62, 1397-1406, http://doi.org/10.1016/s0016-7037 (98)00076-3, 1998.

Smith, C. R., De Leo, F. C., Bernardino, A. F., Sweetman, A. K., and Arbizu, P. M.: Abyssal food limitation, ecosystem structure and climate change, Trends Ecol Evol, 23, 518-528, http://doi.org/10.1016/j.tree.2008.05.002, 2008.

Song, J.: Biogeochemical Processes of Biogenic Elements in China Marginal Seas, Advanced Topics in Science and Technology in China, Springer Berlin, Heidelberg, 662 pp., http://doi.org/https://doi.org/10.1007/978-3-642-04060-3, 2010.

Sun, Q., Song, J., Li, X., Yuan, H., and Wang, Q.: The bacterial diversity and community composition altered in the oxygen minimum zone of the Tropical Western Pacific Ocean, J. Oceanol. Limnol., 39, 1690-1704, http://doi.org/10.1007/s00343-021-0370-0, 2021.

Takahashi, T., Sutherland, S. C., Wanninkhof, R., Sweeney, C., Feely, R. A., Chipman, D. W., Hales, B., Friederich, G., Chavez, F., Sabine, C., Watson, A., Bakker, D. C. E., Schuster, U., Metzl, N., Yoshikawa-Inoue, H., Ishii, M., Midorikawa, T., Nojiri, Y., Körtzinger, A., Steinhoff, T., Hoppema, M., Olafsson, J., Arnarson, T. S., Tilbrook, B., Johannessen, T., Olsen, A., Bellerby, R., Wong, C. S., Delille, B., Bates, N. R., and de Baar, H. J. W.: Climatological mean and decadal change in surface ocean pCO_2, and net sea–air CO_2 flux over the global oceans, Deep Sea Res. Part II Top. Stud. Oceanogr., 56, 554-577, http://doi.org/10.1016/j.dsr2.2008.12.009, 2009.

Thompson, R. O. R. Y.: Climatological Numerical Models of the Surface Mixed Layer of the Ocean, Journal of Physical Oceanography, 6, 496-503, 1976.

Tian, D., Li, X., Song, J., Ma, J, Yuan, H & Duan, L.: Vertical layering and transformation of particulate organic carbon in the tropical Northwestern Pacific Ocean waters based on δ^{13}C, Figshare [Dataset]. https://doi.org/10.6084/m9.figshare.26197808, 2024

Turner, J. T.: Zooplankton fecal pellets, marine snow, phytodetritus and the ocean's biological pump, Prog. Oceanogr., 130, 205-248, http://doi.org/10.1016/j.pocean.2014.08.005, 2015.

563   Walsh, D. A., Zaikova, E., Howes, C. G., Song, Y. C., Wright, J. J., Tringe, S. G., Tortell, P. D., and
564   Hallam, S. J.: Metagenome of a versatile chemolithoautotroph from expanding oceanic dead zones,
565   Science, 326, 578-582, http://doi.org/10.1126/science.1175309, 2009.

566   Wu, L., Liu, Z., Liu, Y., Liu, Q., and Liu, X.: Potential global climatic impacts of the North Pacific Ocean,
567   Geophys. Res. Lett., 32, http://doi.org/10.1029/2005gl024812, 2005.

568   Zeebe, R. E. and Wolf-Gladrow, D.: CO_2 in Seawater: Equilibrium, Kinetics, Isotopes, Elsevier
569   Science2001.

570   Zhong, G., Li, X., Song, J., Qu, B., Wang, F., Wang, Y., Zhang, B., Tian, D., Ma, J., Yuan, H., Duan, L.,
571   Li, N., Wang, Q., and Xing, J.: The increasing big gap of carbon sink between the western and
572   eastern Pacific in the last three decades, Front. Mar. Sci., 9,
573   http://doi.org/10.3389/fmars.2022.1088181, 2022.

574   Zuo, J., Song, J., Yuan, H., Li, X., Li, N., and Duan, L.: Impact of Kuroshio on the dissolved oxygen in
575   the East China Sea region, J. Oceanol. Limnol., 37, 513-524, http://doi.org/10.1007/s00343-019-
576   7389-5, 2018.